Available online at www.sciencedirect.com
ScienceDirect
ELSEVIER
International Journal of Solids and Structures 43 (2006) 5969–5980
INTERNATIONAL JOURNAL OF SOLIDS and STRUCTURES
www.elsevier.com/locate/ijsolstr

Evolution of collective damage in a polyamide 6–silicate nanocomposite

X. Kong, S.S. Chakravarthula, Y. Qiao *

Department of Civil Engineering, University of Akron, Akron, OH 44325-3905, USA

Received 17 May 2005; received in revised form 5 July 2005
Available online 30 August 2005

Abstract

The microvoiding in crack-tip plastic zone in a partly exfoliated polyamide 6–silicate nanocomposite is investigated through the experimental measurement of microvoid size distribution and the computer simulation in context of nonlinear fracture mechanics. In order to analyze the effect of silicate content on fracture resistance, the evolution of the collective microvoids induced by the silicate nanolayers is characterized by the void number density (VND). The influences of the filler–matrix interaction on the yielding and hardening behaviors, as well as the total number, volume fraction, and nucleation and growth rates of microvoids are discussed in detail.

Keywords: Fracture toughness; Microvoiding; Number density

1. Introduction

The superior properties of polyamide 6–silicate nanocomposites, such as high stiffness and strength, low permeability, and high combustion resistance, have made them attractive for a wide variety of engineering applications (Yasue et al., 2000; Masenelli-Varlot et al., 2002; Qiao et al., 2005). Over the past two decades, numerous studies have been performed for the development of processing techniques and material characterization. However, usually as a ''side issue'', the addition of the silicate nanofillers would increase the level of brittleness, which could greatly limit the applicability of these materials in load-bearing components (Giza et al., 2000; Tjong et al., 2002).

* Corresponding author. Tel.: +1 330 972 2426; fax: +1 330 972 6020.
E-mail address: yqiao@uakron.edu (Y. Qiao).

0020-7683/$ - see front matter
doi:10.1016/j.ijsolstr.2005.07.019

Polyamide 6–silicate nanocomposites are obtained by dispersing silicate nanolayers in polyamide 6 matrix. The small thickness of the silicate nanolayers around 1 nm and the relatively large length and width around 100–1000 nm lead to the ultrahigh three-dimensional aspect ratio. A silicate nanolayer contains several sheets of SiO_4 tetrahedral filled by Al^{3+} or Mg^{2+} (Brindley and Brown, 1980). The basic structural unit of silicate minerals is tactoid, consisting of about 100 layers. This layer stack must be disrupted during the nanocomposite processing. Usually the polyamide 6–silicate nanocomposites are synthesized through monomer intercalation technique (Kato and Usuki, 2000; Carrado, 2000). The initial basal distance of the tactoid is around 1 nm, which is smaller than the polymer chains. In polar solvents such as water, the layer stack can swell and the monomers can be intercalated into the interlayer by displacing the Al^{3+} and Mg^{2+} ions. The macromolecules can then be formed through in situ polymerization at appropriate temperature and pressure. The basal distance would be expanded to 10–20 nm and eventually the nanolayers are exfoliated.

In neat polyamide 6, the dominant mechanism of plastic deformation is cold drawing, and under compressive loading shear banding can also take place (Friedrich, 1983). With the addition of the silicate nanolayers, the crystallinity can be either reduced slightly (Wang et al., 2002) or nearly constant (Chan et al., 2002), while the spherulite size is reduced significantly (Tjong et al., 2002), which was attributed to that the nanofillers can promote crystallization nucleation and the molecular mobility in amorphous phase is considerably lowered. At a crack tip, breakdown of individual lamella or layer stacks associated with the nanolayer-induced stress concentration results in the microvoiding near the filler/lamellae–amorphous interface, causing the fibrillation quite similar with that in an amorphous polymer (Gloaguen and Lefebvre, 2001). At room temperature, the critical J-integral, J_{IC}, decreases with the increasing of silicate content, the decreasing of polymer–silicate interface strength, and the reduction in degree of dispersion (Russell and Beaumont, 1980; Nair et al., 2002). As silicate content increases, a ductile-to-brittle transition takes place in the range of 2–7 wt.%. Tjong et al. (2002) reported that the energy at break can be greatly lowered by about 75% and the elongation at break can be reduced from more than 100% to smaller than 30%.

Experimental evidences have shown that, for the polymer–silicate nanocomposites, the fracture toughness is nearly proportional to the plastic zone size, indicating that the plastic deformation mechanism is quite similar in a wide range of silicate content (Nair et al., 2002), probably due to the small void size and the rigidity of the silicate layers. However, currently there is still no satisfactory model that can relate the micromechanisms of fracture to the macroscopic properties. In order to identify the optimum microstructure, the behavior of the silicate nanolayers must be studied quantitatively. In this article we will discuss the evolution of the collective microvoids in context of nonlinear fracture mechanics, with the concept of microvoid number density being incorporated.

2. Experimental

To understand the effect of silicate content on the fracture resistance, four groups of samples were investigated: (1) neat polyamide 6 (N6); (2) polyamide 6–1.7 wt.% silicate nanocomposite (NC17); (3) polyamide 6–3.7 wt.% silicate nanocomposite (NC37); and (4) polyamide 6–5.0 wt.% silicate nanocomposite (NC5). The nanocomposites were provided by the Ube Industrial, Ltd and Dr. M. Kato in the Toyota CRD Lab, Inc. They were produced through the in situ polymerization method discussed by Kato and Usuki (2000), in which synthetic mica tactoids were first mixed with a ε-caprolactam solution at 80 °C and then kept at 220 °C for a relatively long time. Once the basal space expanded to about 2 nm, the temperature was raised to 260 °C. The wide angle X-ray diffraction (WAXD) data showed that the nanolayers were partly exfoliated (Qiao et al., 2005).

The as-received materials were in pellet form with the size around $4 \times 2 \times 2$ mm. After drying at 80 °C for 24 h in a 285A Isotemp vacuum oven, the pellets were compression molded into 0.5 mm thick films using a 3912 Carver hydraulic compression molding machine. The effect of the heat treatment history was removed by keeping the materials at 240 °C for about 8 min followed by air cooling. Tensile samples of the size of $50 \times 10 \times 0.5$ mm were cut from the films. For the fracture experiment, single edge notched specimens (SENS) were produced by pre-notching the tensile samples using a fresh razor blade, with the notch depth of 3.0 mm and the radius of notch root smaller than 0.1 mm.

The tensile and fracture experiments were performed in a type 5569 Instron machine at room temperature. The gauge length was 25 mm and the crosshead speed was set to 1.0 mm/min. The experimental data of the proportional limits $\{\sigma_y, \varepsilon_y\}$ for the samples of different silicate contents, c, are listed in Table 1. Through the experiment on SENS, the critical J-integrals, J_{cr}, and the failure time, t_{cr}, were measured. The results of J_{cr} are shown in Fig. 1.

For NC17 and NC37, the microvoid population were analyzed in a number of nominally identical SENS. The experimental setup was similar with that of the fracture experiment. The tests were stopped at $0.6t_{cr}$ or $0.8t_{cr}$, before the final failure would occur. The specimens were immersed in liquid nitrogen and broken apart cryogenically. The fracture surfaces were coated in an Emitech K575X turbo sputter coater and observed in a Hitachi S2150 SEM. By measuring the radii of the voids in randomly chosen SEM images of crack-tip zones, the size distributions of microvoids were obtained, as shown in Tables 2 and 3.

Table 1
The tensile properties of the polyamide 6–silicate nanocomposites

Nanocomposites	c (wt.%)	σ_y (MPa)	ε_y (%)	m
N6	0.0	49	5.1	–
NC17	1.7	67	4.4	1.2
NC37	3.7	78	2.5	2.0
NC50	5.0	84	1.8	3.7

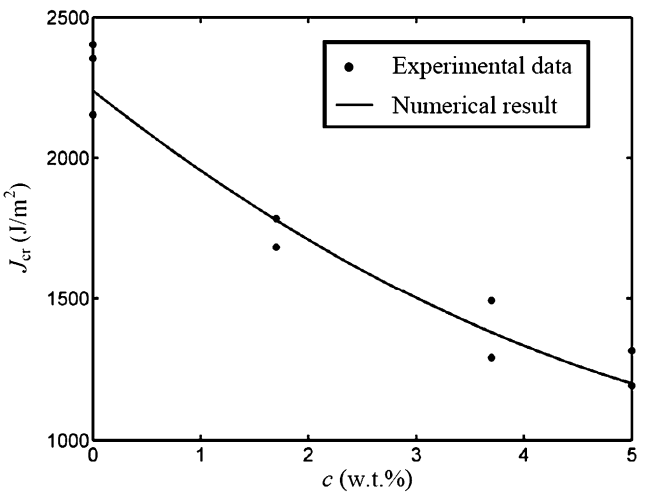

Fig. 1. The critical J-integral of polyamide 6–silicate nanocomposites as a function of the silicate content, c.

Table 2
The size distribution of microvoids in a polyamide 6–1.7% silicate nanocomposite

Time (t/t_{cr})	c_v (%) ($0 < a \leqslant 0.3$ μm)	c_v (%) ($0.3 < a \leqslant 0.6$ μm)	c_v (%) ($0.6 < a \leqslant 1.0$ μm)	c_v (%) ($a > 1.0$ μm)
0.6	71	18	9	2
0.8	69	16	10	5

Table 3
The size distribution of microvoids in a polyamide 6–3.7% silicate nanocomposite

Time (t/t_{cr})	c_v (%) ($0 < a \leqslant 0.3$ μm)	c_v (%) ($0.3 < a \leqslant 0.6$ μm)	c_v (%) ($0.6 < a \leqslant 1.0$ μm)	c_v (%) ($a > 1.0$ μm)
0.6	73	15	10	2
0.8	75	10	11	4

3. Evolution of collective microvoids in crack-tip plastic zone

3.1. Plastic deformation at the crack tip

Fig. 2 shows a typical true stress—true strain curve of polyamide 6–silicate nanocomposites. When the applied strain is relatively small, the material is in the elastic domain (stage I) until the strain exceeds the proportional limit, ε_y. As the deformation increases, in stage II, the material behavior is highly nonlinear and the permanent damage occurs. The silicate nanolayers act as stress concentrators resulting in the somewhat homogeneous microvoiding, especially at the sites where positional and orientational correlation among nanolayers is pronounced. When the strain reaches a critical value ε_s, in stage III, the microvoid nucleation and growth become heterogeneous, associated with fibrillation and local drawing that cause considerable lateral shrinkage and whitening. Eventually, the polymer chains are "straightened" and significant hardening occurs. In this stage local cold drawing dominates the material behavior and the effect of microscale defects is only secondary.

In a precracked sample, since the size of the reinforcements in the nanocomposites is much smaller than the crack-tip plastic zone and the characteristic length of crystallites, the crack-trapping and bridging effects are negligible (Qiao, 2003; Qiao and Kong, 2004). Due to the high degree of strain concentration, in the near-tip field the material behavior would rapidly enter stage III, accompanied by the crack-tip blunting.

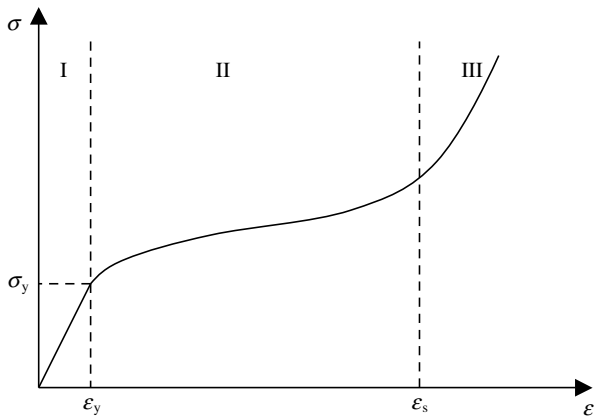

Fig. 2. A typical true stress—true strain curve of the polyamide 6–silicate nanocomposite.

In the far field, but still within the plastic zone, the deformation is in stage II and the evolution of collective microvoids is the dominant process. The microvoids can be formed through the breakdown of lamella or layer stacks, and their growth leads to the final failure of the material (Gloaguen and Lefebvre, 2001; Avlar and Qiao, 2005). Outside the plastic zone the background behavior is elastic and contributes little to the crack growth.

3.2. Growth of a single microvoid

In the microvoiding zone, the stress–strain relation of the nanocomposite can be stated as

$$\sigma_e/\sigma_y = \begin{cases} \varepsilon/\varepsilon_y & \varepsilon \leqslant \varepsilon_y \\ (\varepsilon/\varepsilon_y)^m & \varepsilon_y < \varepsilon \leqslant \varepsilon_s \end{cases} \tag{1}$$

where σ_e is the effective stress and m is a material parameter related to the silicate content, c.

The growth of a spherical void under triaxial loading is essentially one-dimensional. In such a spherical coordinate system the effective strain rate can be defined as

$$\dot{\varepsilon} = 2\dot{r}/r \tag{2}$$

and the effective strain is

$$\varepsilon = 2\ln(r/R) \tag{3}$$

where r and R are the current and initial void radii, respectively. The strain associated with the void growth can then be expressed as $\varepsilon_a = 2\ln(a/a_0)$, i.e.

$$\mathrm{d}\varepsilon_a = 2\frac{a_0}{a}\mathrm{d}a \tag{4}$$

where a is the current void size and a_0 is the initial void size.

The balance of linear momentum gives

$$\frac{\partial\sigma_r}{\partial r} - \frac{2\sigma_e}{r} = 0 \tag{5}$$

with the boundary condition of

$$\sigma_r(r,t) = 0 \quad \text{at } r = a$$
$$\sigma_r \to p_0 \quad \text{at } r \to \infty$$

where p_0 is the transient pressure. Through an integration method (Chung et al., 1987),

$$p_0 = \frac{2}{3}\sigma_y + \int_0^{\varepsilon_a} \frac{\sigma_e}{\exp(3\varepsilon_1/2 + \sigma_e/2G) - 1}\mathrm{d}\varepsilon_1 \tag{6}$$

with $\varepsilon_1 = \varepsilon - \varepsilon_y$, which can be rewritten as

$$\frac{\mathrm{d}p_0}{\mathrm{d}\varepsilon_a} = \frac{\sigma_e}{\exp(3\varepsilon_1/2 + \sigma_e/2G) - 1} \tag{7}$$

Thus, we have

$$\mathrm{d}a = \frac{a}{2a_0}\mathrm{d}\varepsilon_a = \frac{\exp(3\varepsilon_1/2 + \sigma_e/2G) - 1}{\sigma_e}\mathrm{d}p_0 \tag{8}$$

Eq. (8) describes the growth rate of the void subjected to $p_0(t)$, with t being the time. According to a study performed by Wu et al. (2003), this close-form expression works quite well when a/a_0 is smaller than 2–3, which is in consistent with the strain range under consideration.

As depicted in Fig. 3, microvoiding is pronounced only in the far-field. Following the classic HRR theory (Rice and Rosengren, 1968; Hutchinson, 1968), the stress and strain distributions in the microvoiding zone can be stated as

$$\{\sigma_r, \sigma_\theta, \sigma_{r\theta}\} = \sigma_n \widetilde{K}^m r^{-m/(m+1)} \{\tilde{\sigma}_r, \tilde{\sigma}_\theta, \tilde{\sigma}_{r\theta}\} \tag{9}$$

$$\{\varepsilon_r, \varepsilon_\theta, \varepsilon_{r\theta}\} = \varepsilon_n \widetilde{K}^m r^{-m/(m+1)} \{\tilde{\varepsilon}_r, \tilde{\varepsilon}_\theta, \tilde{\varepsilon}_{r\theta}\} \tag{10}$$

where σ_i and ε_i are stress and strain components, respectively $(i = r, \theta, r\theta)$; $\tilde{\sigma}_i$ and $\tilde{\varepsilon}_i$ are dimensionless functions of the rotation angle from the median plane, θ; and

$$\widetilde{K} = \left[\frac{E}{\sigma_y^2}\frac{J}{I(m)}\right]^{\frac{1}{m+1}}$$

with $E = \sigma_n/\varepsilon_n$, J the J-integral, and $I(m)$ a numerical function of m.

During the fracture process where the J-integral keeps increasing, since the macroscopic properties of the material are homogeneous, the effect of unloading at the crack tip is negligible. Thus, the size of the crack-tip plastic zone, r_y, can be estimated through $\sigma_e = \sigma_y$. The boundary of the stretching zone, r_s, is defined by $\varepsilon_e = \varepsilon_s$, with ε_e being the effective strain.

3.3. Evolution of collective microvoids

Consider the fracture experiment in which the J-integral increases from 0 to J_{cr} with a constant rate, $\dot{J}$. Through Eqs. (8)–(10) the growth of a single microvoid at the crack tip can be simulated. However, due to the small size of the silicate nanolayers, the microvoids are much smaller than the plastic zone size, i.e. the

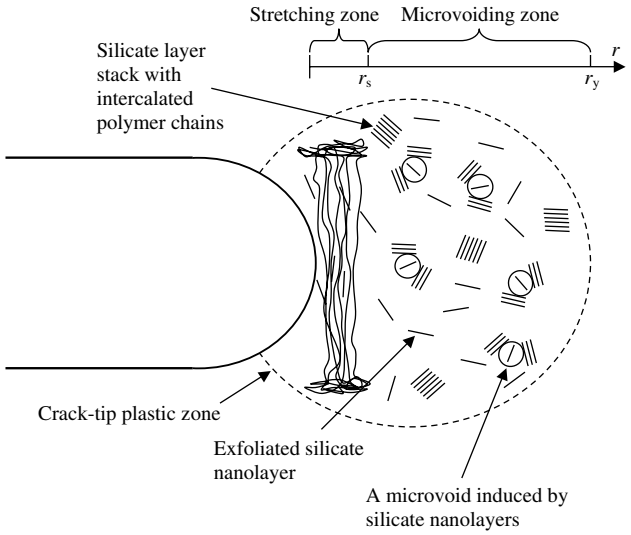

Fig. 3. A schematic diagram of the evolution of collective microvoids in the crack-tip plastic zone.

fracture behavior is dominated by the collective microvoids instead of several large defects. It is, therefore, necessary to discuss the evolution of the microvoid population.

During the early stage of crack-tip damage evolution, the microvoids are far and few between and the nucleation and growth of the microvoids can be assumed isolated. Once the size of a certain portion of the microvoids is close to the void–void spacing, the interaction among the microvoids is pronounced and as a result the homogeneous characteristic of microvoiding is lost. Under this condition, the heterogeneous craze-like fibrillation or local drawing becomes dominant, leading to the eventual macroscale failure. In the current study, the critical J-integral, J_{cr}, is taken as the value at the end of the early stage when the microvoid interaction becomes important. The post-critical plastic deformation will be neglected.

The collective microvoids can be characterized by the void number density (VND), $n(a,t)$, through the equilibrium equation

$$\frac{\partial n(a,t)}{\partial t}+\frac{\partial}{\partial a}[A(a,t)n(a,t)]=n_{\mathrm{N}}(a,t) \tag{11}$$

where $n(a,t)$ is defined as the number of microvoids of size a at time t per unit volume, $A(a,t)$ is the average void growth rate, and $n_{\mathrm{N}}(a,t)$ is the average void nucleation rate, i.e. the number of microvoids of size a that are formed in unit volume per unit time. The concept of defect number density has been applied in studying multiple site and widespread damages for a wide variety of materials quite successfully (Qiao and Hong, 1998; Hong and Qiao, 1999). The second term at LHS of Eq. (11) reflects the influence of void growth, and RHS is the source term. If we assume that all the nucleated microvoids are of the same size, a_0, Eq. (11) can be rewritten as

$$\frac{\partial n(a,t)}{\partial t}+\frac{\partial}{\partial a}[A(a,t)n(a,t)]=0 \tag{12}$$

with the boundary condition of $n(a_0,t)=n^*(t)$ indicating the void nucleation rate. Since under an increasing J the voids will never shrink, we do not need to consider the range of $0<a<a_0$.

The nucleation rate can be stated as

$$n^*(t)=\alpha\cdot(N_0-D_0)\cdot(J/J_0)^{\beta} \tag{13}$$

where α and β are material constants, N_0 is the average filler number per unit volume, and $D_0=\int_0^{\infty}n(a,t)\,\mathrm{d}a$ is the total void number. The value of N_0 can be estimated as $V_{\mathrm{f}}/V_{\mathrm{f0}}$, where V_{f0} is the average volume of a single nanolayer, $V_{\mathrm{f}}=\frac{\rho_{\mathrm{n}}}{\rho_{\mathrm{f}}}.\left(\frac{1}{c}-\frac{\rho_{\mathrm{f}}-\rho_{\mathrm{n}}}{\rho_{\mathrm{f}}}\right)$ is the filler volume fraction, and $\rho_{\mathrm{n}}=1.1\times10^3\ \mathrm{kg/m^3}$ and $\rho_{\mathrm{f}}=3.2\times10^3\ \mathrm{kg/m^3}$ are the weight densities of polyamide 6 and silicate, respectively.

The void growth rate can be obtained through Eq. (8) as

$$A(a,t)=\frac{\mathrm{d}a}{\mathrm{d}J}\dot{J} \tag{14}$$

which, according to Eqs. (7)–(10), is position dependent. In the following discussion, the effective void growth rate $\overline{A}(a,t)$ is taken as the average value of $A(a,t)$ in the microvoiding zone. The critical condition at the onset of heterogeneous damage evolution can be stated as

$$\int_{a_{\mathrm{cr}}}^{\infty}n(a,t)\,\mathrm{d}a\geqslant N_{\mathrm{cr}} \tag{15}$$

that is, there exist at least N_{cr} voids larger than a critical size a_{cr}. For the rapid local drawing to occur, a_{cr} should be close to the average spacing among the microvoids $d_0=(1/D_0)^{1/3}$. In a quasi-FCC structure of the silicate nanolayers, N_{cr} can be taken as $\xi N_0/4$, with ξ being a correction factor. For the homogeneous damage evolution, $\xi=1$.

According to van Es et al. (2000), the modulus of the nanocomposite can be calculated as

$$E = \sigma_n/\varepsilon_n = 0.49E_{\|} + 0.51E_{\perp} \tag{16}$$

where $E_{\|}$ and $E_{\perp}$ are the upper bound and lower bound of the tensile modulus, respectively, which are functions of silicate content and can be obtained through stress/strain average method (e.g. McClintock and Argon, 1993). The Poisson's ratio, v, on the other hand, is quite insensitive to c, and will be taken as 0.38 in the following discussion. Note that the shear modulus $G = E/2(1+v)$.

Finally, the initial condition of $n(a,t)$ can be taken as

$$n(a,0) = 0 \tag{17}$$

i.e. initially the material is defect free. The VND model is now complete. There are two parameters associated with the microvoid nucleation $\{\alpha,\beta\}$ that are still unknown. They must be estimated by comparing the numerical and experimental results. Once their values are determined, Eq. (15) gives the failure time t_{cr}, and then the critical J integral can be obtained as

$$J_{cr} = \int_0^{t_{cr}} \dot{J}\,\mathrm{d}t \tag{18}$$

4. Results and discussion

The experimental results of tensile properties of the nanocomposites are listed in Table 1. As the silicate content c rises, the yield strength increases, which is compatible with the literature data. On the other hand, the extensibility decreases significantly, especially the stretch strain ε_s, i.e. the silicate nanolayers suppress the plastic deformation. This phenomenon is in consistent with that the strain hardening factor, m, increases with c. As a result, the fracture resistance is reduced as more nanofillers are added in the matrix. The experimental data of the tensile properties provide a basis for understanding the role of silicate nanolayers in crack growth. The c dependence of the parameters $\{\sigma_y,\varepsilon_s,m\}$ can be regressed as third-order polynomials.

The measured void size distributions on the cryogenically separated surfaces of NC17 and NC37 at different t/t_{cr} are shown in Tables 2 and 3, with c_v being the fraction of the microvoids with the size in the range under consideration. A correction factor of $\sqrt{2/3}$ was used in the void size calculation to take account for the fact that the fracture plane does not go through the main circle of every void. It can be seen clearly that the n–a relation is a descending curve in both nanocomposites, which should be attributed to that, as the existing microvoids grow larger, new microvoids with the size of a_0 are nucleated continuously and thus $n(a,t)$ is always higher in the lower a range. In both NC17 and NC37, the fraction of voids larger than 1 μm increases nearly 5–6 times as t/t_{cr} rises. While this ratio is quite insensitive to the silicate content, in NC37 the fraction of small voids is somewhat higher than that in NC17, and, accordingly, the fraction of large voids is lower. This phenomenon suggests that the distributed silicate nanolayers can hinder the void growth. In the VND model, this effect is captured by Eq. (16).

By using the VND model established in Section 3.3, the evolution of microvoids can be simulated numerically. It was found that if α is taken as 5.0×10^{-9} and β is set to 2.2, the simulation results of $n(a,t)$ fit with the experimental measurements quite well. As t/t_{cr} increases, the $n(a,t)$ curve keeps moving upwards and toward the higher a end due to the continuous void nucleation and growth (see Fig. 4). Since the nucleation is more important than the growth, in the lower a range $|\mathrm{d}n(a,t)/\mathrm{d}a|$ increases with t, while in the higher a range it decreases, i.e. the evolution of the population of large microvoids is "slower" than that of small ones. Consequently, the failure time defined by Eq. (15), which is dominated by the number density of the microvoids larger than a_{cr}, is nonlinear to the silicate content. The values of α and β are determined

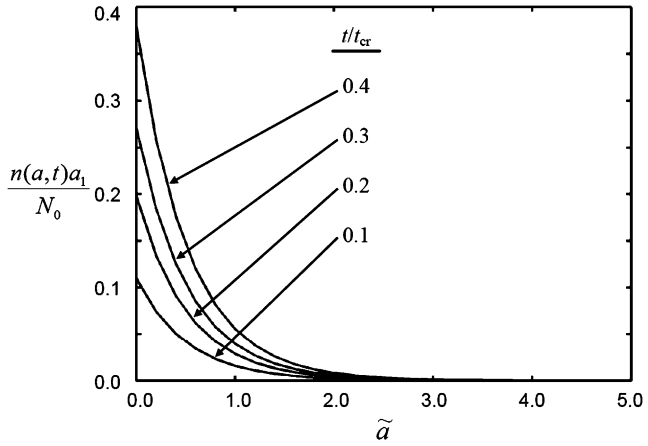

Fig. 4. The evolution of the microvoid number density, $n(a,t)$.

by the fundamental mechanisms and processes that govern the void formation related to the matrix–filler and filler–filler interactions, which should be sensitive to the processing and post-processing treatment techniques. Note that α and β are independent of the silicate content, c. The relatively high α value indicates that in the nanocomposites the void nucleation is relatively easy. On the other hand, the value of β, which is larger than 1, suggests that, as J increases, an increasingly large portion of nanofillers would fail.

Fig. 5 shows the evolution of the total void number, D_0, where the characteristic void number N_1 is the N_0 of NC17. With the constant $\dot{J}$, the nucleation rate increases with time, and consequently D_0 rises with an increasing rate. Furthermore, the more the silicate nanolayers dispersed in the matrix, the higher the number of available void nucleation sites, so does the value of D_0. The evolution of the total volume of the microvoids is shown in Fig. 6, where $D_3(t) = \frac{4\pi}{3}\int_0^\infty n(a,t)a^3\,\mathrm{d}a$. Similar to D_0, both of $\mathrm{d}^2D_3/\mathrm{d}t^2$ and $\mathrm{d}D_3/\mathrm{d}c$ are positive. However, since the void growth rate is lower in the high silicate content nanocomposites, the effect of increasing c on D_3 is less significant.

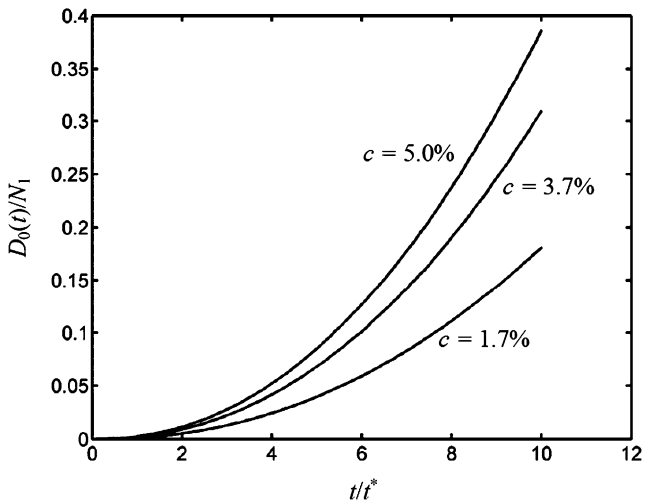

Fig. 5. The evolution of the total microvoid number, D_0.

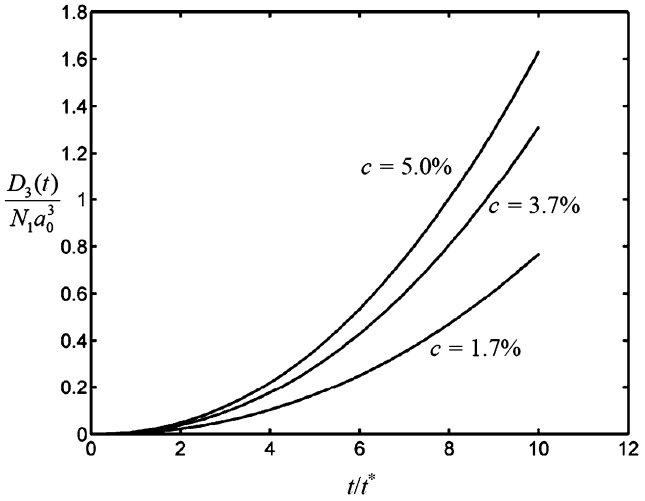

Fig. 6. The evolution of the total volume of microvoids, D_3.

As discussed above, the addition of silicate nanolayers leads to the decrease in void growth rate and the increase in void nucleation rate. According to the analysis of the relationship between the silicate content and the void size distribution, the former, which suppresses the damage evolution at the crack tip, is less important. Therefore, the net result of increasing c is the decrease in fracture resistance. Through Eq. (18), the fracture resistance can be calculated as a function of c, which is shown in Fig. 1. It can be seen that the numerical results of J_{cr} fit with the experimental data quite well.

It is clear that the above discussion provides only a framework for the study on fracture behavior of polyamide 6–silicate nanocomposites. In order to understand the details of the microvoiding process, the fundamental role of silicate nanolayers in the plastic deformation at the crack tip as well as its influence on the matrix properties must be investigated at the molecular level. Note that in the current research the time dependent characteristic of the nanocomposites is ignored.

5. Conclusions

To summarize, the evolution of collective microvoids at the crack tip in polyamide 6–silicate nanocomposites is investigated in the framework of the equilibrium of microvoid number density. Due to the small filler size, the reinforcing mechanisms in conventional composite materials such as crack trapping and bridging are no longer important. The factor of the nanoreinforcements comes in by affecting the crack-tip plastic deformation through microvoiding. The addition of the silicate nanolayers increases the stiffness, and thus suppresses the microvoid growth, while on the other hand it also promotes the microvoid nucleation. The experimental data of the microvoid size distribution indicates that the void nucleation effect is more pronounced, and therefore the fracture resistance is reduced with the increasing of silicate content. The following conclusions are drawn:

(1) At the crack tip in a polyamide 6–silicate nanocomposite, the number of small microvoids is always larger than that of large microvoids.

(2) As the collective microvoids evolve, the fractions of both nanolayer-sized and large-sized microvoids keep increasing; that is, the number density distribution curve becomes steeper in the lower a range and flatter in the higher a range.
(3) The sensitivity of the fracture resistance to the silicate content decreases as the silicate content increases.
(4) The influence of increasing silicate content on the total microvoid number is more pronounced than that on the microvoid volume fraction.

Acknowledgements

This work was supported by the National Science Foundation under Grant No. CMS-0408276. Special thanks are also due to Mr. Savas Avlar for the help with the experiment.

References

Avlar, S., Qiao, Y., 2005. Effects of cooling rate on fracture resistance of polyamide 6–silicate nanocomposites. Composites Part A 36, 624–630.
Brindley, G.W., Brown, G., 1980. Crystal Structures of Clay Minerals and Their X-ray Identification. Mineralogical Society.
Carrado, K.A., 2000. Synthetic organo- and polymer-clays: preparation, characterization, and materials applications. Appl. Clay Sci. 17, 1–23.
Chan, C., Wu, J., Li, J., Cheung, Y., 2002. Polypropylene/calcium carbonate nanocomposites. Polymer 43, 2981–2992.
Chung, D.T., Horgan, C.O., Abeyaratne, R., 1987. A note on a bifurcation problem in finite plasticity related to void nucleation. Int. J. Solids Struct. 23, 983–988.
Friedrich, K., 1983. Crazes and shear bands in semi-crystalline thermoplastics. Adv. Polym. Sci. 52/53, 226–274.
Giza, E., Ito, H., Kikutani, T., Okui, N., 2000. Fiber structure formation in high-speed melt spinning of polyamide 6/clay hybrid nanocomposites. J. Macromol. Sci. Phys. B39, 545–559.
Gloaguen, J.M., Lefebvre, J.M., 2001. Plastic deformation behavior of thermoplastic-clay nanocomposites. Polymer 42, 5841–5847.
Hong, Y., Qiao, Y., 1999. An analysis on overall crack-number-density of short fatigue cracks. Mech. Mater. 31, 525–534.
Hutchinson, J.W., 1968. Singular behavior at the end of a tensile crack in a hardening material. J. Mech. Phys. Solids 16, 13–31.
Kato, M., Usuki, A., 2000. Polymer-clay nanocomposites. In: Pinnavaia, T.J., Beall, G.W. (Eds.), Polymer-Clay Nanocomposites. John Wiley & Sons, pp. 97–110.
Masenelli-Varlot, K., Reynaud, E., Vigier, G., Varlet, J., 2002. Mechanical properties of clay-reinforced polyamide. J. Polym. Sci. B40, 272–283.
McClintock, F.A., Argon, A.S., 1993. Mechanical behavior of materials. CBLS, Marietta, OH.
Nair, S.V., Goettler, L.A., Lysek, B.A., 2002. Toughness of nanoscale and multiscale polyamide-6,6 composites. Polym. Eng. Sci. 42, 1872–1882.
Qiao, Y., 2003. Fracture toughness of composite materials reinforced by debondable particulates. Scripta Mater. 49, 491–496.
Qiao, Y., Avlar, S., Chakravarthula, S.S., 2005. Essential fracture work of nylon 6–silicate nanocomposites. J. Appl. Polym. Sci. 95, 815–819.
Qiao, Y., Hong, Y., 1998. An analysis of collective damage for short fatigue cracks based on equilibrium of crack number density. Eng. Fract. Mech. 59, 151–163.
Qiao, Y., Kong, X., 2004. Unstable crack advance across a regular array of short fibers in brittle matrix. Compos. Sci. Technol. 64, 711–717.
Rice, J.R., Rosengren, G.F., 1968. Plane strain deformation near a crack tip in a power law hardening material. J. Mech. Phys. Solids 16, 1–12.
Russell, D.P., Beaumont, P.W.R., 1980. Structure and properties of injection-molded polyamide-6, parts 1, 2, 3. J. Mater. Sci. 15, 197–221.
Tjong, S.C., Meng, Y.Z., Xu, Y., 2002. Structure and properties of polyamide-6/vermiculite nanocomposites prepared by direct melt compounding. J. Polym. Sci. B40, 2860–2870.
van Es, M., Xiqiao, F., van Turnhout, J., van der Giessen, E., 2000. Comparing polymer-clay nanocomposites with conventional composites using composite modeling. In: Proc. 9th Int. Conf. Additives, April 10–12, 2000. pp. 391–413.

Wang, K.H., Choi, M.H., Koo, C.M., Xu, M., Chung, I.J., Jang, M.C., Choi, S.W., Song, H.H., 2002. Morphology and physical properties of polyethylene/silicate nanocomposite prepared by melt intercalation. J. Polym. Sci. B40, 1454–1463.

Wu, X.Y., Ramesh, K.T., Wright, T.W., 2003. The dynamic growth of a single void in a viscoplastic material under transient hydrostatic loading. J. Mech. Phys. Solids 51, 1–26.

Yasue, K., Katahira, S., Yoshikawa, S., Fujimoto, K., 2000. In situ polymerization route to polyamide 6-clay nanocomposites. In: Pinnavaia, T.J., Beall, G.W. (Eds.), Polymer-Clay Nanocomposites. John Wiley & Sons, pp. 111–126.